Radiating and nonradiating behavior of hyperbolic-secant, raised-cosine, and Gaussian input light pulses in dispersion-managed fiber systems

C. M. Ngabireng,* P. Tchofo Dinda, and A. Tonello

Laboratoire de physique de l'Université de Bourgogne, UMR CNRS No. 5027, Avenue A. Savary, Boîte Postale 47 870, 21078 Dijon Cédex, France

K. Nakkeeran[†]

Department of Engineering, Fraser Noble Building, King's College, University of Aberdeen, Aberdeen AB24 3UE, United Kingdom

P. K. A. Wai

Photonics Research Center and Department of Electronic and Information Engineering, The Hong Kong Polytechnic University, Hung Hom, Kowloon, Hong Kong

T. C. Kofane

Laboratoire de Mécanique de l'Université de Yaoundé I, Boîte Postale 812, Yaoundé I, Cameroon

We address the problem of optical light pulses, called dressed pulses, which do not match the stationary pulse profile of a dispersion-managed (DM) fiber system and we theoretically analyze the associated radiation. Comparing hyperbolic-secant, raised-cosine, and Gaussian pulse envelopes, we show that the general radiation figure is highly sensitive to the input pulse profile. As common general features for these pulse profiles, we find a rich variety of dynamical states that includes weak-, moderate-, and strong-radiation states, depending on the map strength of the DM fiber system. We demonstrate the existence of two intervals of map strengths where the emitted radiation is of considerably low level. The first interval falls in a region of small map strengths where pulses are weakly dressed. In contrast, the second window of low radiation appears in the map strength region corresponding to strongly dressed pulses. As a major difference with respect to the pulse profile, we find that light pulses with Gaussian input profile produce less radiation in the fiber system than hyperbolic-secant or raised-cosine pulses can do. In particular, at the lower edge of the second window of low radiation, Gaussian light pulses with large initial dressing acquire the best ability to execute a stable nonradiative propagation over transoceanic distances.

I. INTRODUCTION

A major feature of the forthcoming generation of optical transmission systems (OTSs) lies in the use of dispersion management, that is, an appropriate concatenation of fiber segments with alternation of positive and negative group-velocity dispersion throughout the transmission line [1]. The main advantage of DM lines is the robustness of the transmitted signal upon a large variety of perturbations [1]. Nonetheless, the related stationary solutions possess in general nontrivial temporal profiles can be hardly matched by light pulses of commercial laser sources [1,2]. Commercial optical sources, indeed, cannot generate ultrashort light pulses having both a high repetition rate (160 GHz or more) and a temporal profile of sufficiently high quality to ensure data transmission in advanced DM transmission systems. Consequently, light pulses that are routinely used for developing such systems cannot match exactly the desired stationary profile. Although DM fiber systems are known to be tolerant

to relatively small offsets of amplitude or chirp [1], the transmission performances are remarkably compromised when the pulse profile deviates from the stationary solution. A light pulse whose shape is detuned from the exact shape of the stationary pulse is called a "dressed pulse," and the *dressing field* measures the residual field that should be added to the input pulse field to obtain the exact stationary pulse.

Light pulses in practice are more or less dressed according to the particular DM fiber system configuration. Now, it is a well known fact that if a dressed pulse is launched in a fiber system, it may spontaneously radiate away a certain amount of energy, while propagating in the DM fiber system [3–8]. Through the emission of radiation, the pulse attempts to evolve towards a stationary profile. In an OTS, the amount of radiation may grow substantially owing to the presence of a large number of pulses in the transmission system, and therefore, may cause distortions in the pulse shape. The serious practical difficulties to generate ultrashort pulses that can match complex profiles, put into the evidence of the radiation phenomenon as a limiting factor for the performances of future OTSs.

Recently, a spectral analysis has been used to obtain the global picture of the radiating behavior of a solitary Gaussian-shaped light pulse in DM fiber systems [7]. Various

———

*Permanent address: ENSP, University of Yaoundé I, Yaoundé I, Cameroon.

[†]Electronic address: k.nakkeeran@abdn.ac.uk

types of radiating behaviors have been found, including *weak-*, *moderate-*, or *strong-radiation* states depending on the map strength of the DM fiber system. In particular, the existence has been established of a critical map strength where Gaussian pulse of large initial dressing executes a solitonlike propagation, without emitting radiation over transoceanic distances. In reality, the behavior of a solitary pulse cannot coincide with that of a pulse embedded in a bit pattern. In a real OTS, the emission of radiation by a given pulse may be influenced not only by the radiation coming from other pulses but also by pulse-to-pulse interactions. This fact has motivated a recent study of the radiating behavior of trains of closely packed Gaussian light pulses in dispersion-managed OTSs [8]. In Ref. [8], we have described the similarities and some fundamental differences between the radiating behavior of a solitary pulse and that of a pulse train. In particular we have shown that for small map strengths, short sequences of pulses strongly emit radiation, and the total amount of radiated energy increases linearly with the number of pulses in the sequence. Here we want to point out that previous studies have exclusively focused on input pulses with Gaussian profile [7,8]. However, the generation of Gaussian-shaped pulses suitable for high bit rate is difficult [9,10]. For instance, the output of the commonly used Mach-Zehnder pulse carvers is rather close to raised-cosine (RC) profiled pulses. For completeness, besides Gaussian and RC profile pulses, one can consider an hyperbolic-secant (sech) profiled pulses, which is the well-known exact soliton solution in an ideal lossless fiber with constant (anomalous) dispersion [11]. Considering the three types of pulses just mentioned, where self-phase-modulation exactly balances the anomalous group-velocity dispersion, one can ask the following question: how sensitive is the radiation emission with respect to the variations of the input pulse profile? A related question would be the following: Among the results of the previous studies based on Gaussian profile assumption [7,8], are there some general properties related to the characteristic of the transmission line (and not to the specific pulse shape)?

In the present paper, we attempt to answer these questions by performing a comparative numerical study of the radiating and nonradiating behavior of optical pulses in DM fiber systems, in which we employ sech and RC input pulse profiles. Our analysis reveals the general features of the radiation phenomenon in DM fiber systems, and the radiation pictures related to the specific input pulse profile.

The paper is organized as follows. In Sec. II, we present the OTS under consideration, the governing equation, as well as some general qualitative considerations. In Sec. III we present the radiation properties of solitary pulses. In Sec. IV we present the radiation picture of short trains of pulses, and a comparison with the solitary pulse behavior. Also in Sec. IV we analyze the quality of transmission of pulse trains as a function of the map strength, and we draw our conclusions in Sec. V.

II. EQUATIONS AND GENERAL QUALITATIVE CONSIDERATIONS

Pulse propagation in a periodically amplified DM fiber system can be described by the following nonlinear Schrödinger equation (NLSE):

$$\psi_z + i\frac{\beta(z)}{2}\psi_{tt} - i\gamma|\psi|^2\psi - \frac{\alpha}{2}\psi + \mathcal{A}[\psi] = 0, \qquad (1)$$

where $\psi(z,t)$ is the electric field envelope at position z in the fiber and at time t. β, γ, and α represent group-velocity dispersion, self-phase-modulation, and loss parameters, respectively. The operator $\mathcal{A}$ accounts for the action of amplifiers which are used to compensate the fiber losses. Hereafter we consider a densely dispersion-managed (DDM) fiber system, that is, a DM fiber line in which the period of the dispersion swing (map length) is a fraction of the amplifier span of the system [12]. The DDM fiber systems allow small pulse breathing and hence reduce the single-channel pulse-to-pulse interactions. Pulse breathing and transmission performances of the DDM fiber systems are closely related to the map strength S defined by $S=(L_+\beta_+-L_-\beta_-)/T_0^2$, where T_0 is the full width at half maximum (FWHM) pulse width at chirp-free point, β_+ (β_-) and L_+ (L_-), respectively, represent the normal (anomalous) fiber dispersion parameter and length. In this study we have chosen a pulse width of $T_0 = 1.17$ ps. The dispersion map consists of nonzero dispersion-shifted fibers, with the following typical parameters: dispersion $D^{\pm}=\pm1.5$ ps/nm/km, losses $\alpha^{\pm} = 0.2$ dB/km, effective core area $A_{\text{eff}}^{\pm}=55$ μm^2. The fiber lengths $L_{\pm}$ have been determined using a recently developed analytical design procedure for the DDM fiber systems [13].

III. RADIATING AND NONRADIATING STATES OF SOLITARY WAVES

A. Stationary pulse

Here it is worth recalling that there is no analytical method available to derive the exact soliton solution of a DM fiber system. More specifically, there is no analytical method to obtain the asymptotic stationary DM soliton solution for a given input pulse. Consequently, all the available methods are based on numerical procedures. For example, if one simply lets an initial arbitrary pulse propagate over a sufficiently long distance and removes any extra energy radiated out of the pulse during propagation, then the pulse will evolve itself to an *asymptotic stationary profile* that corresponds to a DM soliton solution. But this *brute force approach* is too time consuming and is therefore seldom used in practice. To accelerate the process of determining the fixed point of a DM fiber system, Nijhof *et al.* [14] have proposed a numerical averaging method, which is commonly used by most researchers working in the field of DM fiber systems. The catch however is that the fixed point solution obtained using this averaging method for a given initial pulse may not coincide with the *asymptotic stationary solution* corresponding to the same initial pulse. As it is difficult to obtain the asymptotic stationary solution of the DM fiber system for a desired initial pulse, in this work we use the fixed point resulting from the averaging method. Hereafter the term *stationary pulse* refers to such a fixed point solution. Similarly, the meaning of the term dressing field used in this work is also not defined in its actual sense with respect to the asymptotic stationary solution, but is defined rather as the
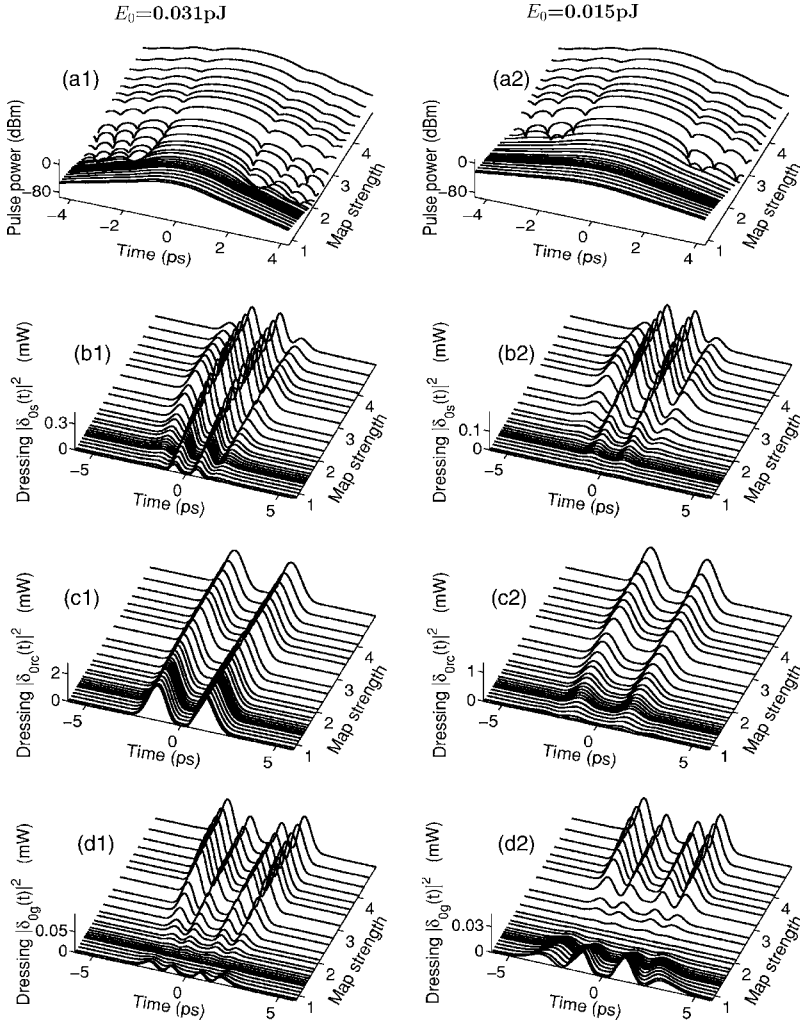
FIG. 1. (a1),(a2) Temporal profiles of the stationary pulse. (b1),(b2) Temporal profiles of the dressing for the sech *Ansatz*. (c1),(c2) RC *Ansatz*. (d1),(d2) Gaussian *Ansatz*.

difference between the stationary pulse and the desired input pulse field.

Using the above mentioned methods [13,14], a general picture displaying the temporal profiles of stationary pulses in a relatively large range of map strengths ($0.85 \leqslant S \leqslant 5$) was obtained in previous study [8]. Here, for completeness we have displayed that general picture in Figs. 1(a1) and 1(a2), which show the power profiles of stationary pulses (DM solitons), for pulse energies of $E_0 = 0.031$ and 0.015 pJ, respectively [8]. In Figs. 1(a1) and 1(a2) one can clearly appreciate the large variety and complexity of the stationary solutions (here plotted in logarithmic scale) especially for large map strengths S, where the principal core is surrounded by several lateral lobes of low intensity. Similar features have been observed in a lossless DM fiber system [1,2].

B. Soliton dressing

Considering the results given in Figs. 1(a1) and 1(a2) one can raise the following question: which analytic profile is the closest to the stationary solution in the map strength region under consideration? A fair answer to this question can be obtained by using a collective-variable technique [15]. To this purpose, one can decompose the stationary solution, hereafter called ψ_{st}, in the following way:

$$\psi_{st} = f_A(x_1, x_2, x_3, x_4, t) + q_A(t), \qquad (2)$$

where the x_i are the collective variables, which represent the fundamental parameters of the pulse. f_A is trial function (often called *Ansatz*) which can be one of the three analytical functions we have mentioned above. Those are

$$f_s = x_1 \operatorname{sech}\left(\frac{t}{x_2}\right)\exp\left(\frac{ix_3 t^2}{2} + ix_4\right), \qquad (3a)$$

$$f_{rc} = \frac{x_1}{2}\left[1 + \cos\left(\frac{\pi t}{x_2}\right)\right]\exp\left(\frac{ix_3 t^2}{2} + ix_4\right), \qquad (3b)$$

$$f_g = x_1 \exp\left(\frac{-t^2}{x_2^2} + \frac{ix_3 t^2}{2} + ix_4\right). \qquad (3c)$$

Here x_1, x_2, $x_3/(2\pi)$, and x_4 represent the amplitude, pulse width, chirp, and phase, respectively. The related FWHM, maxima of pulse power are $\sqrt{2 \ln 2} x_2$, $x_2/\sqrt{2}$, $2x_2 \cos^{-1}(\sqrt{2} - 1)/\pi$, for the Gaussian, sech, and RC *Ansätze*, respectively. The field q_A in Eq. (2) is the residual field. After the choice of the *Ansatz* function, we should minimize the residual field to obtain the best approximation of ψ_{st} using f_A. The mini-

mization procedure is achieved by satisfying the following constraint:

$$C_j = \int_{-\infty}^{\infty} \text{Re}\left(q_A \frac{\partial f_A^*}{\partial x_j}\right) dt = 0 \quad (j = 1, \ldots, 4), \qquad (4)$$

which forces f_A to be the best fit of ψ_{st}. In Eq. (4) the symbol Re represents the real part of the quantity in parentheses. The parameter set x_{j0} ($j=1,\ldots,4$) that satisfies Eqs. (4), determines [from Eqs. (3a)–(3c)] the *Ansatz* f_A corresponding to the best approximation of the stationary pulse. With the knowledge of f_A we can then obtain the following soliton dressing:

$$\delta_{0A} \equiv \psi_{\text{st}} - f_A(x_{10}, x_{20}, x_{30}, x_{40}, t). \qquad (5)$$

A related quantitative measure is the dressing energy $E_{\delta 0A}$, defined as

$$E_{\delta 0A} \equiv \int_{-\infty}^{\infty} |\delta_{0A}|^2 \, dt. \qquad (6)$$

Using the above collective variable approach we have obtained the results shown in Figs. 1(b1), 1(b2), 1(c1), and 1(c2), where we report the power of the dressing fields $|\delta_{0s}|^2$ and $|\delta_{0rc}|^2$, for the sech and RC *Ansätze*, respectively. Figures 1(d1) and 1(d2), show, for comparison, the power of the dressing field $|\delta_{0g}|^2$ for the Gaussian *Ansatz* reported in Ref. [8]. A careful inspection of these figures puts into evidence the following peculiar aspects.

(1) Whatever be the map strength and pulse *Ansatz*, the minimization procedure always ends up with a nonzero residual field. This confirms the already mentioned fact that the DM soliton does not correspond to any one of the three analytic functions of our study.

(2) If we exclude the case of RC pulses of large energy [see Fig. 1(c1)], we find that the amplitude of the dressing field depends strongly on the map strength.

(3) At low pulse energy (e.g., $E_0=0.015$ pJ) $|\delta_{0s}|^2$ decreases to zero for decreasingly small values of S, as can be seen in Fig. 1(b2). This fact is a clear indication that the shape of the DM soliton tends toward a sech profile as S decreases.

(4) The Gaussian *Ansatz* appears as the best fitting function in a relatively large region of map strength: $1<S<2.5$. For $E_0=0.031$ pJ the optimum range of map strength lies around $S=1.45$ [as Fig. 1(d1) shows], whereas for $E_0=0.015$ pJ it appears around $S=2$ [as Fig. 1(d2) shows].

(5) The RC function turns out to be the one having the largest dressing, for any pulse energy or map strength.

The above mentioned characteristics are also clearly evident from Figs. 2, where we show the dressing energy as a function of the map strength S. Moreover, we observe that for large values of S, sech and Gaussian pulses exhibit a similar behavior, having a maximum dressing near $S=4$. In contrast, for small values of S and low pulse energy the behavior of the sech profile becomes rather close to that of the RC pulse, with a dressing energy decreasing monotonically as S diminishes [see Figs. 2(a2) and 2(b2)].

On the other hand, the standard procedure for designing DM transmission systems is fundamentally based on *weakly*
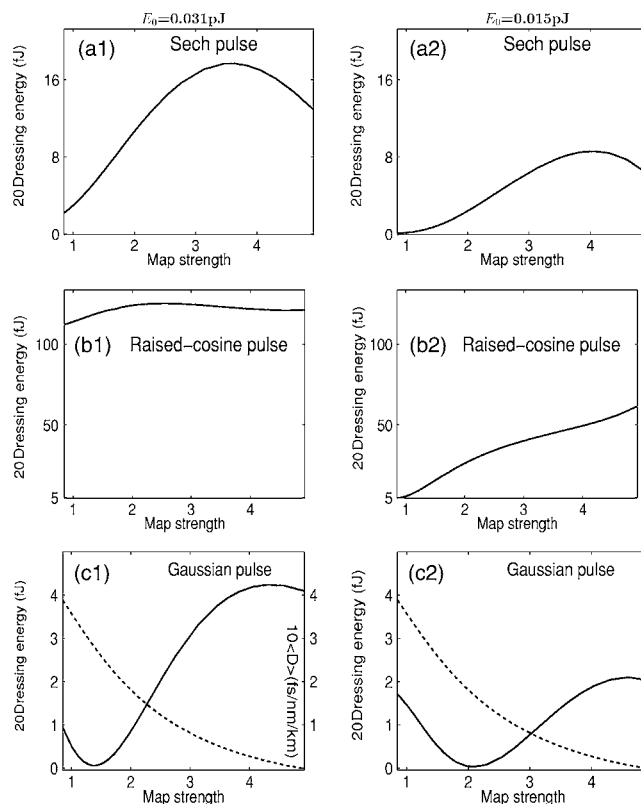

FIG. 2. Dressing energy (solid curve) and average dispersion (dashed line) versus map strength S.

dressed pulses [1,13,16,17]. For example, if we were to conceive a transmission system using Gaussian input pulses, the map strength would be $S\sim1.45$ for a pulse energy of $E_0=0.031$ pJ [see Fig. 2(c1)], or $S\sim2$ for $E_0=0.015$ pJ [see Fig. 2(c2)]. The use of sech input pulses would require designing the system at the lowest available value of S [see Figs. 2(a1) and 2(a2)]. This last choice is severely limited by practical reasons, since the basic dispersion map length must be significantly curtailed to reduce S, thus implying a consequent concatenation of a quite large quantity of fiber segments to cover each amplification span. This last solution is technically more complex and consequently less appealing from an economical standpoint. Figure 2(b2) shows that RC pulses are not immunized against this problem, exhibiting a dressing function much larger than that of the other two profiles.

Figures 2(a1), 2(b1), and 2(c1) show that at high energy, the Gaussian *Ansatz* yields the smallest dressing at any map strengths. For a weaker pulse energy, the magnitude of the dressing can be lowered by using either a Gaussian profile (with $S\sim2$) or a sech profile (with $S=S_{\text{min}}=0.85$).

C. Radiating and nonradiating dynamical states

It is crucial to realize that the use of an input pulse of a given shape f_A instead of the exact stationary pulse ψ_{st} causes the injection of an initial perturbation $\delta_{0A}(t)$ in the transmission system. In other words, the dressing $\delta_{0A}(t)$ may be seen as an initial perturbation, which may develop a perturbing field along the transmission line, say,

$$\delta_A(z,t) = \psi_{st} - \psi(z,t), \tag{7}$$

where $\psi(z,t)$ is the NLSE solution using f_A as input condition. The field $\delta_A(z,t)$, which represents the soliton dressing at distance z and time t, can be decomposed in the following way:

$$\delta_A(z,t) = \delta_{As}(z,t) + \delta_{Ad}(z,t). \tag{8}$$

The term δ_{As} represents the dressing component with zero frequency (measured from the transmission frequency), whereas the term δ_{Ad} incorporates all the nonzero frequency components of the dressing. Hence δ_{As} represents a static component with respect to the pulse's rest frame (localized field). A nonzero field δ_{As} corresponds to a situation where a reshaping process that takes place in the beginning of the dynamics, in which the pulse definitely looses its initial shape and converges towards a different stationary DM soliton. The field δ_{Ad} represents the dynamical components of the dressing (with respect to the pulse's rest frame), that is, the radiated field.

In the present work, we have used a pulse width of T_0 = 1.17 ps, which corresponds to a bit rate of 160 gigabits/s, with a bit window of T_{TB}=6.25 ps. Now, temporal supports of sech or Gaussian functions are not strictly bounded within a bit window; in consequence the ratio $T_{TB}/T_0 \sim 5$ is not representative enough for the entire pulse energy. We then define the radiation energy as the energy that falls outside a temporal window of two adjacent bit slots:

$$E_R(z) \equiv \int_{-\infty}^{+\infty} |\delta_{Ad}|^2 \, dt \approx \int_{-\infty}^{-T_{TB}} |\psi|^2 \, dt + \int_{T_{TB}}^{+\infty} |\psi|^2 \, dt. \tag{9}$$

Figures 3 show the picture of the radiated energy at different propagation distances z (1000, 3000, and 6000 km). This picture unveils a host of dynamical states, which exhibit both some common features and some qualitative differences among the three input conditions under consideration.

Common features of the radiation pictures can be summarized as follows.

(1) We clearly see in the radiation curves of Figs. 3 the existence of two windows of low radiation located around the map strengths denoted as S_{op1} and S_{op2}, respectively. The two optimum map strengths S_{op1} and S_{op2} are pinpointed in the region of low ($S<2.3$) and large values of S ($S>2.3$). When $S \sim S_{op1}$ (first window of low radiation), the pulses emit a weak residual radiation, whereas more astonishingly, when $S \sim S_{op2}$, the pulse propagation is totally nonradiating. In other words, we can say that around this map strength window ($S \sim S_{op2}$), the nonradiating pulse with initial large dressing with respect to the initial *stationary solution*, might be converging to an asymptotic solution different from the solution given by the averaging technique.

(2) For sufficiently large propagation distances, the radiation figure converges to a single curve (see Figs. 3 at z = 6000 km), which does not match the curve of the dressing energy in Figs. 2. Moreover, we observe from Figs. 3 and 2 that the second window of low radiation ($S \sim S_{op2}$) falls in the region of maximum initial dressing. This result is fundamentally important since it refutes the general idea that the
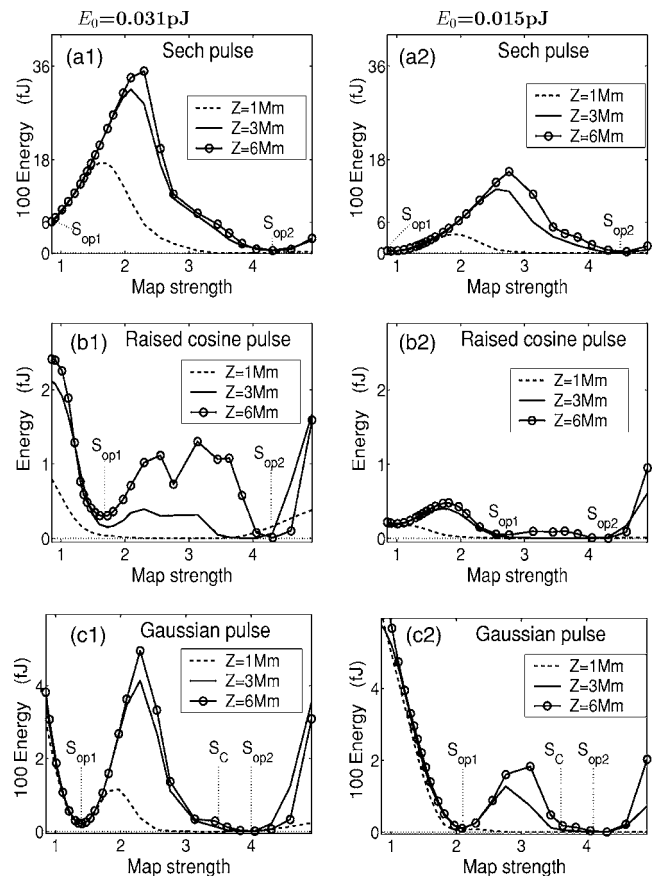

FIG. 3. Radiated energy versus map strength.

magnitude of radiation is closely related to the magnitude of the initial dressing. Thus our result shows that in a DM fiber system, the amplitude of the initial dressing does not necessarily determine the quantity of energy that will be radiated during the pulse propagation in the transmission system.

(3) The quantity of radiated energy appears as being much strongly related to the map strength and the particular shape of the input pulse. It is therefore conceptually possible to control the radiation process through an optimization of the map strength S.

(4) Both the qualitative and quantitative analysis show that the importance of the radiation process is closely related to the level of the pulse energy.

The items mentioned above, that are common for the three pulse profiles, might be seen as being the characteristics of the DM fiber line. On the other hand, Figs. 3 show some differences with respect to the input pulse shape.

(1) For a Gaussian input pulse, the first window of low radiation is found to be very sensitive to the energy level of the pulse, whereas for a sech pulse S_{op1} is systematically located at the lower bound of S, which is here set to 0.85.

(2) Whatever be the map strength, the RC input pulse radiates much stronger than the Gaussian or sech pulses. Except for excessively small map strengths, Gaussian input pulses are less radiating than the sech pulses.

(3) For the map strength $S=4.9$, the quantity defined in Eq. (6), which has been treated so far as being the radiated energy, tends to settle to dramatically high levels, as Figs. 3
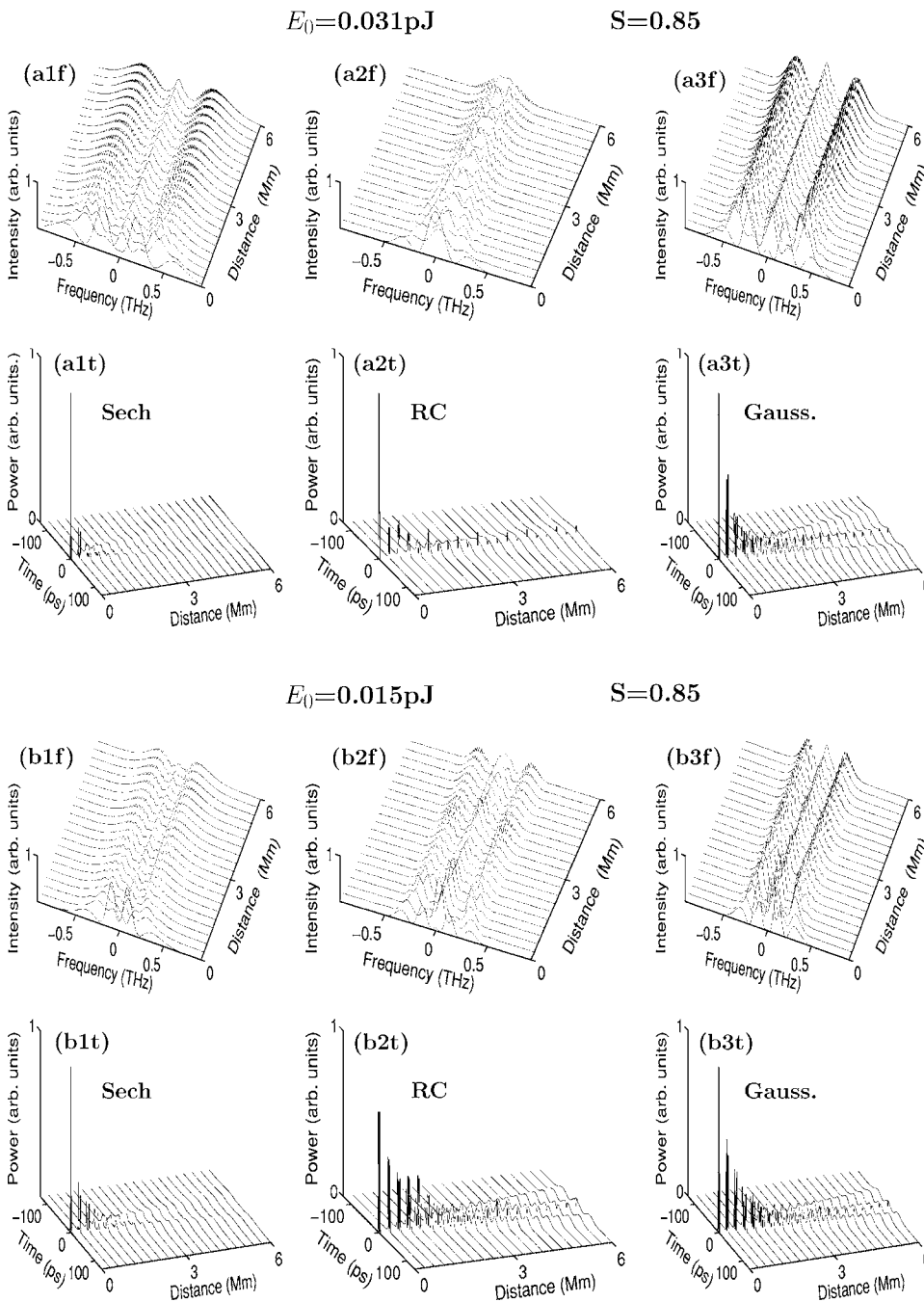
E_0=0.031pJ   S=0.85

FIG. 4. Evolution of the dressing field as a function of the propagation distance for $S=0.85$.

E_0=0.015pJ   S=0.85

show. Rigorously, this behavior does not correspond to a radiation process, but reflects rather a general degradation of the quality of the propagation, in which the temporal pulse shape is less and less localized within its initial time slot.

Thus, we have obtained a quite general view of the soliton radiation as a function of the map strength. More light can be shed on this view by including some fundamental properties of the radiation spectrum shape. In doing so we have scrutinized the evolution of dressing for different pulse types, and this study unveils both dissimilarities and common points among the three *Ansätze* of our study.

Common points are listed below.

(1) For weak map strengths the dressing spectrum acquires both a zero-frequency component (static component) and a set of components with a nonzero offset from the carrier frequency (causing radiation). The static component is clearly visible in Figs. 4(a1f), 4(a2f), and 4(a3f), which we have obtained for $S=0.85$. It is worth noting that the presence of a nonradiating component is an indication that the pulse will converge to a state that differs from the initial (or reference) stationary pulse. On the other hand, a careful inspection of the spectra of Figs. 4(a1f), 4(a2f), and 4(a3f) and 4(b1f), 4(b2f), and 4(b3f) reveals two regimes in the pulse dynamics: As soon as the dynamics begin, the pulse enters a *transient regime* in which a strong reshaping process takes place, leading to a drastic evolution of the pulse spectrum. The transient regime takes place over a relatively short propagation distance, of the order of a tenth of an amplifier
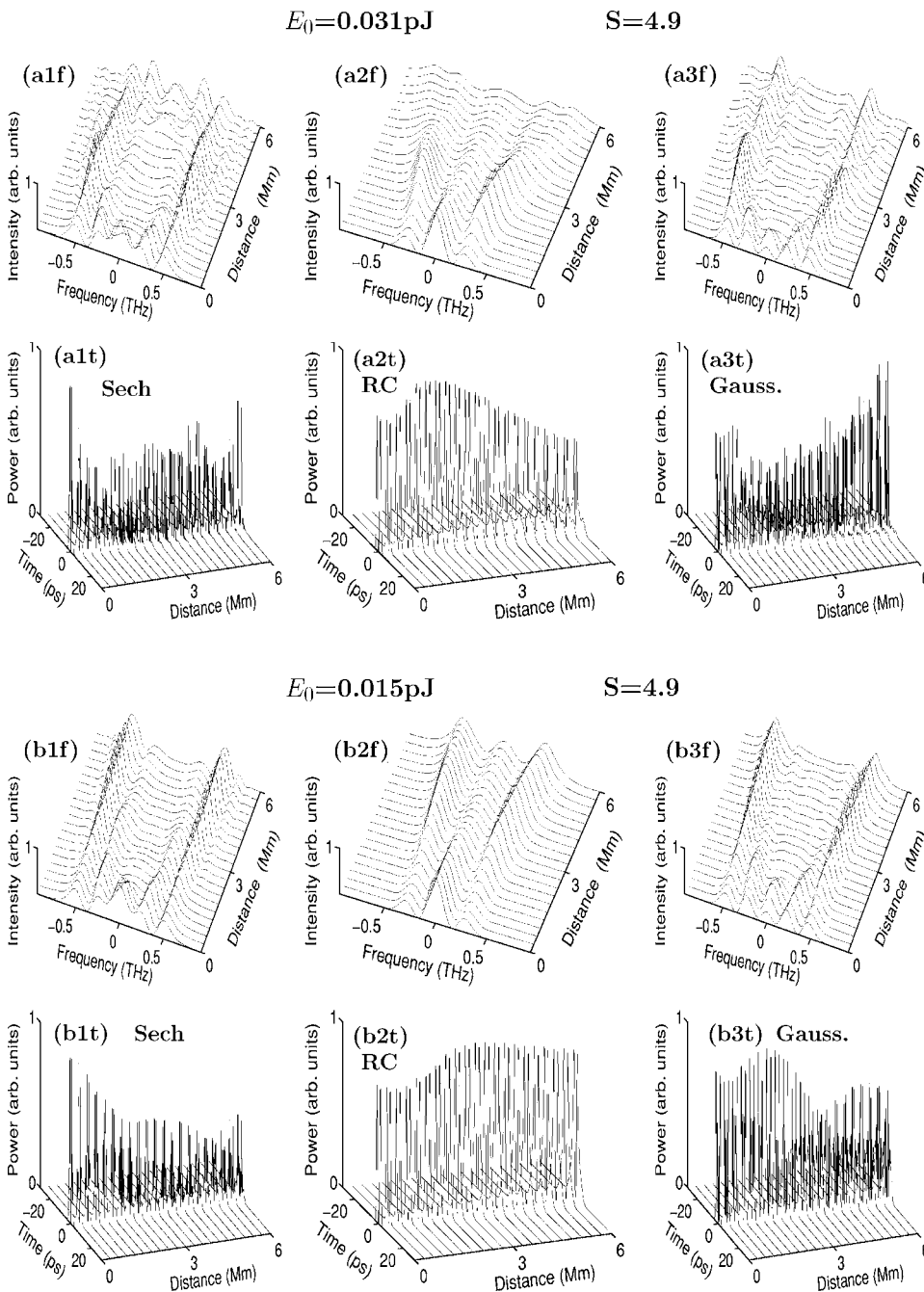
$E_0=0.031$pJ   S=4.9

FIG. 5. Evolution of the dressing field as a function of the propagation distance for $S=4.9$.

$E_0=0.015$pJ   S=4.9

span. Then the pulse accedes to a *quasipermanent regime*, where the spectrum does not undergo significant changes over long distances (several thousands of kilometers). On the other hand, one can clearly observe in Figs. 4(a1t), 4(a2t), and 4(a3t) and 4(b1t), 4(b2t), and 4(b3t), a decay of the dressing power leading to an emission of radiation away from the center of the pulse's rest frame. This confirms the important property that the region of very low map strength corresponds to strongly radiating states for the three pulse wave forms of our study.

(2) The second circumstance arises for large values of S, where the three pulse wave forms display similar dynamics. Figures 5, which we have obtained for $S=4.9$, exhibit a completely different behavior in comparison with that of Figs. 4. Indeed, the pulse dynamics for $S=4.9$ exhibits a spectral deg-

radiation throughout the pulse propagation, as can be seen in Figs. 5(a1f), 5(a2f), and 5(a3f) and 5(b1f), 5(b2f), and 5(b3f). This spectral degradation is converted into temporal degradation, as Figs. 5(a1t), 5(a2t), and 5(a3t) and 5(b1t), 5(b2t), and 5(b3t) show, with a pulse wave form spreading out of the initial time slot of the pulse instead of generating a radiation.

In between the two limiting behaviors ($S=0.85$ and 4.9), we have found several dynamical states that change according to pulse energy and initial profile. Figures 6, which we obtained for the map strength $S=1.53$ (located in first window of low radiation for Gaussian pulses), illustrate this large variety of dynamical behaviors. Indeed, one can observe in Fig. 6(a3f) that for $E_0=0.031$ pJ, the Gaussian pulse generates only nonzero-frequency components, whereas for
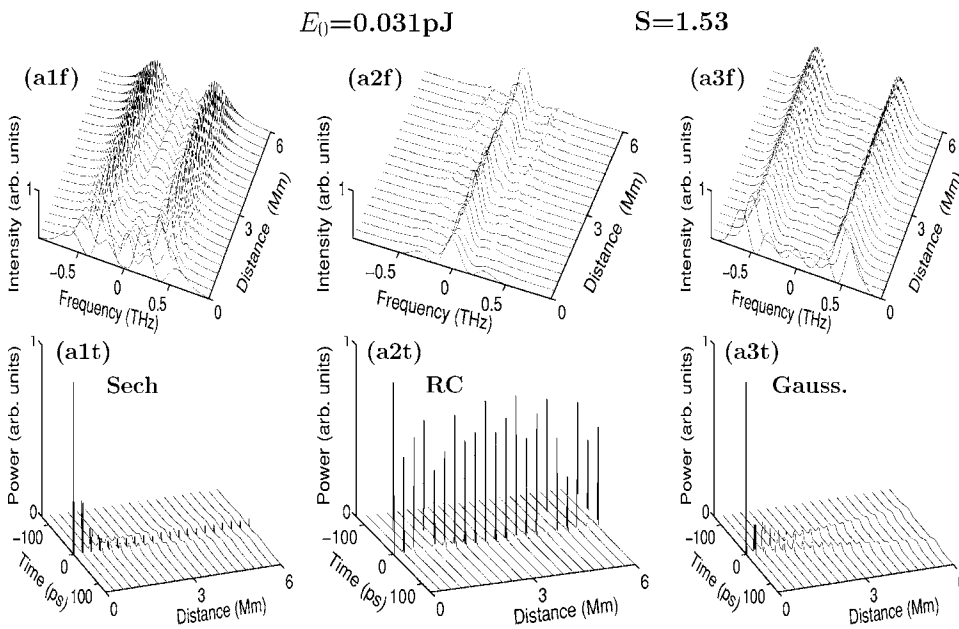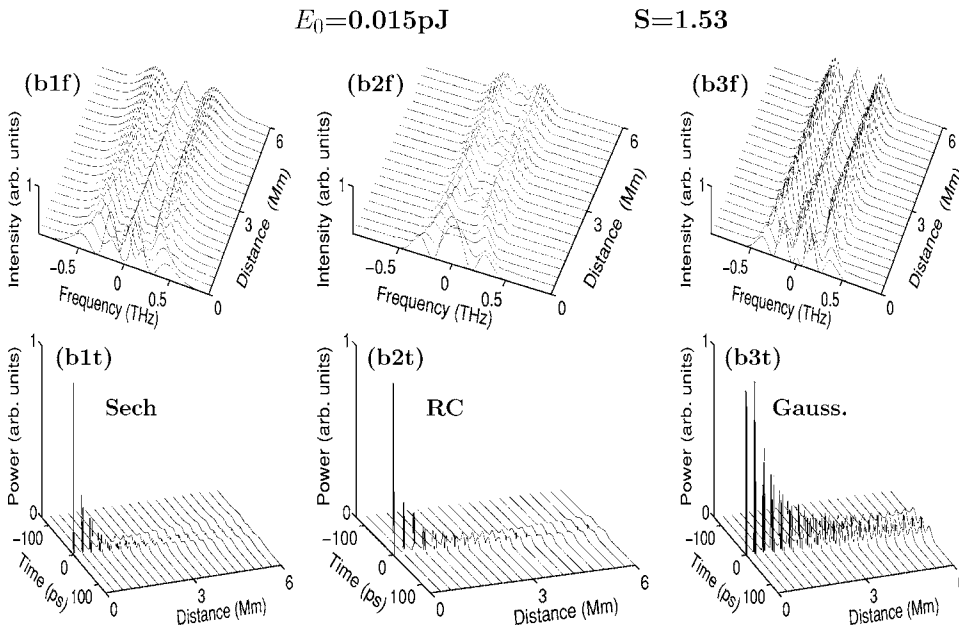
$E_0 = 0.031 \text{pJ}$ S=1.53

FIG. 6. Evolution of the dressing field as a function of the propagation distance for $S = 1.53$.

$E_0 = 0.015 \text{pJ}$ S=1.53

$E_0 = 0.015$ pJ both zero- and nonzero-frequency components are generated [as Fig. 6(b3f) shows]. In contrast, the sech pulses generate both zero- and nonzero-frequency components, for any of the two levels of pulse energy under consideration [see Figs. 6(a1f) and 6(b1f)]. But the greatest qualitative difference comes from the behavior of the RC pulse, which generates only nonzero frequency components at low pulse energy [as Fig. 6(b2f) shows], whereas only a zero-frequency component is significantly generated at high pulse energy [see Fig. 6(a2f)].

On the other hand, Figs. 7, which we obtained for S = 3.6 (that corresponds to the lower edge of the second window of low radiation for Gaussian pulses) exhibit both some qualitative differences and some similar features between the three types of pulse wave forms. Indeed, one can observe that at high energy, both sech and RC pulses are nonradiating

[see Figs. 7(a1t) and 7(a2t)] but they exhibit a poor ability to maintain their initial spectral profile at high energy. In contrast, Gaussian pulses propagate without significant distortions in the dressing spectrum [as Figs. 7(a3f) and 7(b3f) show] and no radiation [as Figs. 7(a3t) and 7(b3t) show]. This dynamics corresponds to a *solitonlike* behavior [7]. To explain the existence of the nonradiative solitonlike behavior one may invoke a previous work by Lakoba *et al.* [3], who demonstrated the existence of internal modes in a lossless DM fiber system. In particular, they showed that an initial dressing having a shape close to that of an internal mode can be trapped within the pulse over very long distances [3]. This solitonlike behavior, which was already mentioned in previous work [7], suggests the existence of such internal modes in the pulse dynamics, and a close proximity of the initial dressing at $S = 3.6$ with one such mode. Other possible expla-
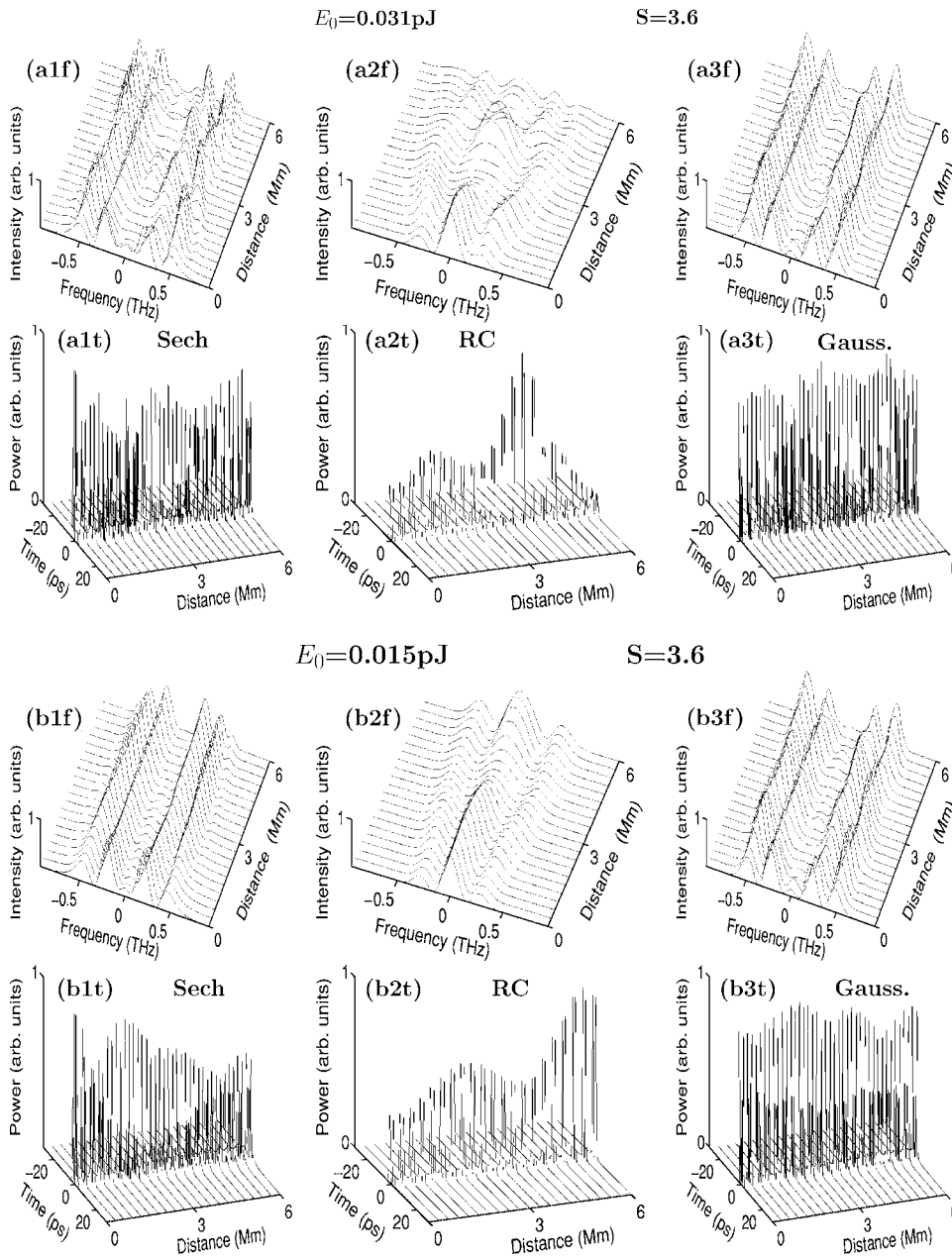
$E_0=0.031\text{pJ}$ $S=3.6$

(a1f) (a2f) (a3f)

(a1t) Sech (a2t) RC (a3t) Gauss.

FIG. 7. Evolution of the dressing field as a function of the propagation distance for $S=3.6$.

$E_0=0.015\text{pJ}$ $S=3.6$

(b1f) (b2f) (b3f)

(b1t) Sech (b2t) RC (b3t) Gauss.

nation could be that the nonradiating pulse with large initial dressing around the second map strength window might be converging to a stationary solution different from that given by the numerical averaging method. More detailed study on the asymptotic stationary solution of the DM fiber system and the stationary solution obtained by the averaging method for the same initial pulse around this map strength window might shed more light on this strange dynamics of the nonradiating behavior of these largely dressed pulses.

On the other hand it is worth noting that at low energy, all the three types of pulses exhibit a clear tendency to maintain their input spectrum, with a better ability for the Gaussian pulse.

On the other hand, we have found that the behavior just described for $S=3.6$ is essentially the same as for other map strength values lying in the second window of low radiation. But as S increases above 4.0, in a very progressive manner

the pulse shape executes variations with increasingly large amplitudes, and there, the pulses become less and less stable, and their energies become less and less localized in time.

IV. RADIATING AND NONRADIATING STATES FOR PULSE TRAINS

A. Radiation energy

Let us take into consideration the radiation of a pulse train, since in optical fiber communications, the information stream is physically reproduced by a synchronized combination of marks and spaces, where each pulse may emit and may be influenced at the same time by radiation from neighboring pulses. Here we extend our previous definition of the radiation energy to a train of N pulses, by assuming that essentially all the energy of the N pulses is initially located in

FIG. 8. Evolution of the average energy radiated per pulse as a function of propagation distance, for sech profiled input pulses.
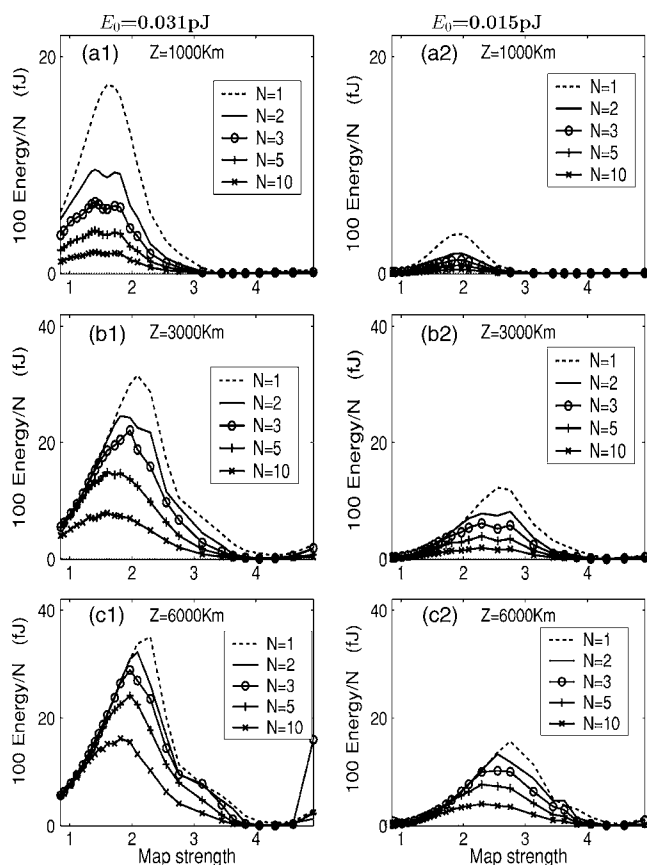

FIG. 9. Evolution of the average energy radiated per pulse as a function of propagation distance, for RC profiled input pulses.

the following temporal window $-NT_{BS}/2-T_{BS}/2 \leq t \leq NT_{BS}/2+T_{BS}/2$. We then define the *radiation energy* E_{RN} for a train of N pulses as the energy that falls in the complementary region of $-NT_{BS}/2-T_{BS}/2 \leq t \leq NT_{BS}/2+T_{BS}/2$:

$$E_{RN} \equiv \int_{-\infty}^{-(NT_{BS}/2+T_{BS}/2)} |\psi|^2 \, dt + \int_{NT_{BS}/2+T_{BS}/2}^{\infty} |\psi|^2 \, dt. \tag{10}$$

Figures 8 and 9 show the quantity E_{RN}/N, which represents the (average) radiation energy per pulse as a function of S, for the sech and RC input pulse profiles, respectively.

Three important items can be noticed from these figures.

(1) After propagation over a sufficiently long distance, the radiation picture for a pulse train exhibits two windows of low radiation, which coincide with those mentioned above for a solitary pulse, as Figs. 8(c1), 8(c2), 9(c1), and 9(c2) show.

(2) In the initial stage of propagation [Figs. 8(a1), 8(a2), 9(a1), and 9(a2)] E_{RN}/N is lower than the energy radiated by a solitary pulse E_{R1} [dashed curves in Figs. 8(a1), 8(a2), 9(a1), and 9(a2)]. Then, as the propagation distance increases E_{RN}/N gradually approaches the same level as E_{R1} [see Figs. 8(b1), 8(b2), 9(b1), and 9(b2)] and for a sufficiently long distance $E_{RN}/N \sim E_{R1}$ [see Figs. 8(c1), 8(c2), 9(c1), and 9(c2)]. In other words, over a transoceanic transmission distance, small trains of N pulses (with $N \leq 5$) radiate an energy
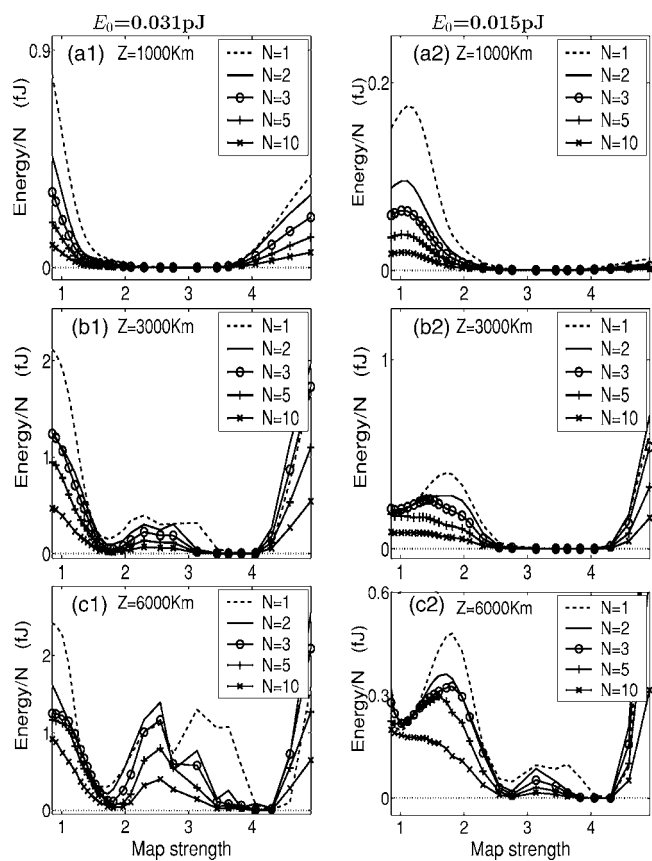
comparable to N times the energy radiated by a single pulse. Consequently we can conclude that in the region of strong radiation the energy radiated by each pulse passes through the adjacent pulses without being captured (without hybridization with the other pulses).

(3) The radiation energy per pulse E_{RN}/N quickly approaches E_{R1} as the number of bits N decreases.

The three items mentioned above for the sech and RC input pulses are similar to the main general features reported in our previous work for a Gaussian input pulse [8].

B. Transmission penalties

A useful conclusion that emerges from our study is that the radiation effects can be avoided conceiving dispersion maps for nonradiating dynamics in the two windows of low radiation, that is, $S \sim S_{op1}$ or $S \sim S_{op2}$. In particular, the window around S_{op2}, where the detected radiation is extremely low, seems to be an eligible choice for transmissions. However radiation is not the unique source of penalties in an OTS, and in general, the optimum system parameters result from a trade off among different factors. In each basic cell of the dispersion map the temporal overlap that arises from pulse breathing may cause four-wave mixing and generate ghost pulses in the zero location [18], thus degrading the transmission quality. It is also a well known fact that the effects of pulse interactions grow strongly for large values of S. Now, the second window of low radiation ($S \sim S_{op2} \approx 4$) is

TABLE I. Quality factor for transmissions of PRBS sequences of 64 pulses.

E (pJ)	S	0.85	**1.45**	**2.3**	**3.4**	3.6	4.05	4.9
0.031	sech	23.5	24.3	26.6	7.1	7.4	3.7	2.2
0.031	RC	6.3	6.4	7.4	1.5	2.3	0	0
0.031	Gauss.	25.9	*131.8*	76.7	*12.4*	11.5	5.6	2.1
0.015	sech	0	29.3	21.2	30.0	24.1	10.8	5.1
0.015	RC	0	11.0	15.0	5.0	3.3	3.0	3.4
0.015	Gauss.	0	32.0	*108.0*	*77.4*	65.7	16.9	8.2

located nearby the highest map strength values that we have considered in our study, whereas S_{op1} is located nearby the lower limit of the same region. The pulse broadening factor a, defined as the ratio between the maximum pulse width and minimum pulse width, is two times larger for $S=4$ ($a \sim 3$) than for $S=S_{op1}<2.0$. In other words, for $S=S_{op2}$ the radiation is indeed reduced to the lowest level but at the expense of large interactions that might overshadow the penalties caused by radiation.

It is therefore interesting to examine whether the second window of low radiation permits a transmission quality that is comparable to that of the first window (which happens to be the unique region that has been privileged so far in the design of OTSs to minimize the initial dressing). To this end we have performed numerical simulations using a pseudo-random binary sequence (PRBS) of 64 elements. In our simulations we have not included the amplifier noises and we have evaluated the quality of transmission by means of the Q factor defined as follows:

$$Q = \frac{|\mu_1 - \mu_0|}{\sigma_1 + \sigma_0}, \qquad (11)$$

where μ_1, μ_0, σ_1, and σ_0 identify the mean values and standard deviations of ones and zeros respectively measured at the center of each time slot. We summarize our results in Table I. We can draw the following conclusions:

It is clear from Table I that for the DDM fiber systems, the Gaussian pulse gives clearly the best performances among the three pulse shapes under consideration. The optimum working point for that pulse corresponds to the largest energy value $E=0.031$ pJ and map strength $S=1.45$ (where we have obtained $Q=131.8$). For $E=0.015$ pJ Gaussian pulses still achieve the best performance but with a map strength of $S \sim 2.3$. For both energy levels the best performance is achieved in the first window of low radiation. Considering these performances, in what follows, we mainly focus on the dynamics of the Gaussian pulses.

The most original outcome of the present set of numerical simulations deals with transmission lines having S in the region $3.4 \leqslant S_C \leqslant 3.6$, which corresponds to the lower edge of the second window of low radiation. We have observed indeed for $E=0.031$ pJ that there is one order of magnitude drop in the Q factor when passing from the system with $S=1.45$ to the system with $S=S_C=3.4$: $Q(S_{op1})/Q(S_C)=131.8/12.42=10.6$. However, for $E=0.015$ pJ that ratio re-

duces to $Q(S_{op1})/Q(S_C)=108/77.4=1.4$. This result suggests that ultralong transmission distances (12 000 km) are possible for pulses which are strongly dressed ($S=S_C$), whereas all the already existing techniques for designing OTSs have systematically privileged weakly dressed pulses ($S \sim S_{op1}$). The map strength $S=S_C$, which lies in the border between radiating and non-radiating states [see Figs. 3(c1) and 3(c2)], permits a solitonlike bearing for the slowly varying dynamics, that is a pulse that does not suffer significant degradations of its shape during propagation. The only drawback in using the map strength $S=S_C$ is its relatively large broadening factor, which may enhance pulse interactions and may explain the modest performance ($Q=12.4$) obtained at high energy $E=0.031$ pJ. In contrast, low energy pulses ($E=0.015$ pJ) having a reduced interaction effects and less radiation, lead to substantial improvement of system performance for $S=S_C$ ($Q=77.4$). From these results, it is clear that the second window of low radiation corresponds to strongly dressed light pulses that can execute highly stable propagation over transoceanic distances.

V. CONCLUSION

To conclude, in this work, we have obtained a general picture of the radiating and non-radiating states of sech and RC light pulses in DM fiber systems. This radiation picture is made up of a rich variety of radiation states, including weak-, moderate-, or strong-radiation states, depending on the map strength of the DM fiber system. Comparing the light pulses having hyperbolic-secant, raised-cosine, and Gaussian input profiles, we have found, as common features, the existence of two windows of low radiation located around the map strengths $S=S_{op1} \sim 1.5$ and $S_{op2} \sim 4$, with a quite surprising fact that the second window ($S=4$) corresponds to the strongly dressed pulses. We have observed these windows of low radiation not only in the behavior of solitary pulses but also in the behavior of small sequences of pulses. We have found that the regions below the first window and between the two windows of low radiation, cause strong radiation, and there, the total amount of radiated energy increases linearly with the number of pulses propagating in the transmission system. The region above the second window of low radiation corresponds to highly unstable propagation. On the other hand, we have found that light pulses with input Gaussian shape produce less radiation than in the case of sech or RC input profile. In particular, the lower edge of the second window of low radiation, that is $S=S_C \sim 3.5$, leads to strongly dressed Gaussian pulses that can execute highly stable propagation over transoceanic distances. This result suggests that a more careful attention should be given to those strongly dressed pulses, which may represent an alternative way to soften severe constraints that are imposed on the pulse shapes capable of being used as information carriers in future optical communication systems.

[1] V. E. Zakharov and S. Wabnitz, *Optical Solitons: Theoretical Challenges and Industrial Perspectives* (Springer-Verlag, Berlin, 1998).

[2] M. J. Ablowitz and G. Biondini, Opt. Lett. **23**, 1668 (1998).

[3] T. I. Lakoba and D. E. Pelinovsky, Chaos **10**, 539 (2000).

[4] T. S. Yang and W. L. Kath, Physica D **149**, 80 (2001).

[5] Y. Chung, V. V. Lebedev, and S. S. Vergeles, Opt. Lett. **29**, 1245 (2004).

[6] D. E. Pelinovsky and J. Yang, SIAM J. Appl. Math. **64**, 1360 (2004).

[7] C. M. Ngabireng and P. Tchofo Dinda, Opt. Lett. **30**, 595 (2005).

[8] C. M. Ngabireng, P. Tchofo Dinda, K. Nakkeeran, and P. K. A. Wai, Opt. Commun. **250**, 24 (2005).

[9] S. Pitois, J. Fatome, and G. Millot, Opt. Lett. **27**, 1729 (2002).

[10] P. Tchofo Dinda, A. Labruyère, J. Fatome, K. Nakkeeran, A. B. Moubissi, S. Pitois, and G. Millot, Ann. Telecommun. **58**, 1785 (2003).

[11] A. Hasegawa and F. Tappert, Appl. Phys. Lett. **23**, 142 (1973).

[12] A. H. Liang, H. Toda, and A. Hasegawa, Opt. Lett. **24**, 799 (1999).

[13] K. Nakkeeran, Y. H. C. Kwan, P. K. A. Wai, A. Labruyere, P. Tchofo Dinda, and A. B. Moubissi, J. Opt. Soc. Am. B **21**, 1901 (2004).

[14] J. Nijhof, W. Forysiak, and N. Doran, IEEE J. Sel. Top. Quantum Electron. **6**, 330 (2000).

[15] P. Tchofo Dinda, A. B. Moubissi, and K. Nakkeeran, Phys. Rev. E **64**, 016608 (2001).

[16] M. Nakazawa, H. Kubota, K. Suzuki, and E. Yamada, Chaos **10**, 486 (2000).

[17] M. Nakazawa, H. Kubota, K. Suzuki, E. Yamada, and A. Sahara, IEEE J. Sel. Top. Quantum Electron. **6**, 363 (2000).

[18] M. J. Ablowitz and T. Hirooka, Opt. Lett. **25**, 1750 (2000).